

Five months in the life of an oceanic eddy: carbon flux and oxygen demand

Alberto Baudena^{1,*}, [...], Rainer Kiko¹

August 10, 2022

¹Sorbonne Université, CNRS, Laboratoire d’Océanographie de Villefranche,
²UMR 7093 LOV, Villefranche-sur-Mer, France
³*To whom correspondence should be addressed;
⁴E-mail: alberto.baudena@gmail.com.

Abstract

Abstract here

1 Introduction

1.1 Oceanic carbon dynamics during times of global change

Global change impacts the distribution and activity of marine life at local to
basin-wide scales, with major consequences for oceanic oxygen (O_2) dynamics,
nutrient cycles and the transfer of CO_2 from the atmosphere to the deep sea.
also include link to oxygen cycle

1.2 Mesoscale activity - a major unknown in oceanic carbon dynamics

Marina Levy

1.3 Carbon flux and turnover estimates - optical instruments enable mesoscale assessments

d'all Olmo, Wineglass effect, ...

We here report on a BGC Argo float - equipped with T, S, O_2 , Chl a, bbp
sensors and a UVP6 - that was deliberately released in a cyclonic eddy off
South Africa. The float was trapped inside this eddy for more than 5 months,
allowing us to target the same water mass and to analyse the carbon and oxygen

²⁴ dynamics in a Lagrangian fashion. To our knowledge this is the first deployment
²⁵ of a BGC Argo float equipped in this fashion in an eddy. We explore this data
²⁶ to ???

²⁷ 2 Results

²⁸ 2.1 Initial characterisation and dynamics of the eddy

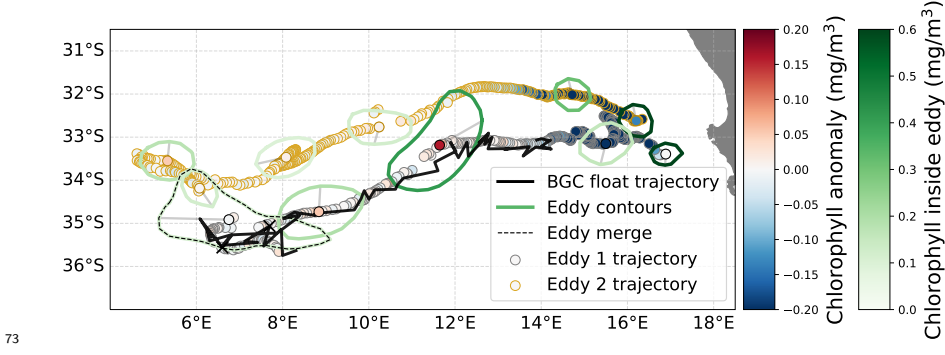
²⁹ 2.1.1 Short overview of eddy and float history

³⁰ Analysis of satellite data indicates that the targeted cyclonic eddy formed on
³¹ the 18 October 2020 at 33.39°S, 16.89°E, 120 km off Cape Columbine (South
³² Africa; Fig. 1). At this time, it had a maximal-velocity radius (Subsec. 4.2,
³³ hereafter radius) of \sim 29.1 km. The mean eddy radius and velocity were $60.2 \pm$
³⁴ 18.8 km and 0.51 ± 0.15 m/s, respectively. In comparison with the mean
³⁵ characteristics of the cyclones originating in the same region (radius: $63.4 \pm$
³⁶ 22.2 km; velocity: 0.30 ± 0.19 m/s; Ioannou et al., 2022), our cyclone was at
³⁷ least 1.5 times stronger. The maximum velocity reached by this cyclone was
³⁸ 0.90 m s^{-1} , which was larger than two cyclones documented in the same region
³⁹ (Ioannou et al., 2022), and close to an intense cyclone described in Manta et al.
⁴⁰ (2021).

⁴¹ The BGC Argo float remained inside the eddy until the 23 September 2021,
⁴² almost always remaining within a distance from the eddy center of about half
⁴³ the radius or less (\sim 23.4 km; Fig. 2a). On the 13 April 2021 when the float was
⁴⁴ released in the eddy at 33.14°S, 13.96°E the eddy radius was \sim 44.7 km (Fig.
⁴⁵ 2a). This was corroborated by analysis of vessel mounted ADCP data analysis,
⁴⁶ which also indicated that the eddy extended down to \sim 750 m (Supplementary
⁴⁷ Fig. S1). After the float left the eddy, it persisted until the ???.

⁴⁸ 2.1.2 Eddy subduction

⁴⁹ The eddy showed a negative temperature anomaly (calculated with respect to
⁵⁰ World Ocean Atlas xxxx-xxxx climatology; Subsec. 4.3) of \sim xx° between the
⁵¹ mixed layer (Methods) and \sim 600 m depth (Supplementary Fig. S5). The depth
⁵² associated with the strongest negative anomaly (\sim -6°) steadily decreased from
⁵³ \sim 290 to \sim 400 m between the 13 April and the 23 September 2021. During the
⁵⁴ same time window, the temperature at 200 m increased from 8.10° to 9.93°,
⁵⁵ and from 4.55° to 5.09° at 500 m (Supplementary Fig. S6). These suggest
⁵⁶ that the eddy subducted during the time window considered, a common process
⁵⁷ among eddies, especially in our study region (REF Artemis and Remi papers
⁵⁸ etc). Therefore, in the following, we will analyse water layers comprised between
⁵⁹ two isopycnal values rather than two isodepth values. In this way, we will follow
⁶⁰ the temporal evolution of the water mass sampled by the BGC Argo float by
⁶¹ taking into account its vertical subduction.



73
 74 Figure 1: Trajectory of the BGC Argo float (solid black line) between the 13
 75 April and the 23 September 2021. The gray-edged filled circles represent the
 76 trajectory of the cyclone (Eddy 1) inside which the BGC Argo float was trapped.
 77 This eddy merged with a cyclone (Eddy 2; trajectory indicated by gold-edged
 78 filled circles) between the 1 and the 11 August 2021. The merging region is
 79 indicated by a black dashed contour centered at $\sim 7^\circ\text{E}$, 35°S . The color of each
 80 circle is proportional to the eddy chlorophyll *a* anomaly (blue and red scale at
 81 right). Four eddy contours are represented as solid lines for Eddy 1 and five
 82 for Eddy 2, colored proportionally to the mean chlorophyll inside them (green
 83 scale at right). Each eddy contour is linked to its corresponding center by a
 84 gray solid line. The black crosses represent the BGC Argo profiles which were
 85 excluded from our analyses.

62 2.1.3 Eddy merging

63 The targeted eddy merged with a cyclone between the 1–11 August 2021. Satellite
 64 analyses showed a merging of the eddy contours, followed by a change of direction
 65 in the targeted eddy (from westward to eastward; Supplementary Video
 66 xx). Signatures of this event were visible as a decrease of salinity and an in-
 67 crease of temperature and oxygen after the eddy merging event (Subsec. 2.2
 68 and Supplementary Sec. 5.1). The shifts in temperature and salinity during
 69 this time period are consistently larger than those observed in other isolated
 70 eddies, suggesting that they were caused by the merging of the two eddies.
 71 Therefore, in the following we will refer to the cyclone targeted by the float as
 72 Eddy 1, and to the cyclone which merged with it as Eddy 2.

Rémi can
you please
indicate how
much and
add a REF

87 2.1.4 Eddy chlorophyll *a* contents from satellite data

88 Satellite data analysis identifies a positive chlorophyll *a* anomaly in Eddy 1 at
 89 the beginning of its life, compared to the surrounding area between the margin of
 90 Eddy 1 (at a given day) and a circle four-times the mean eddy radius, ~ 368 km
 91 (Supplementary Fig. S8). Eddy 1 originated in a coastal region in October 2020,
 92 trapping chlorophyll *a* rich waters ($\simeq 0.76 \text{ mg/m}^3$). In the following months,
 93 the chlorophyll *a* concentration inside Eddy 1 declined, while the surrounding

94 region continued to show high chlorophyll *a* values. About two weeks before the
95 float deployment the chlorophyll *a* values in the surrounding area also declined
96 to values that were very similar to the chlorophyll *a* values inside the eddy.
97 Eddy 2 showed a story similar to Eddy 1. It originated in September 2020
98 in a coastal region nearby (~ 150 km far North-West) and it moved westward
99 until merging with Eddy 1. It trapped chlorophyll *a* rich waters upon formation
100 (~ 0.61 mg/m³), which then declined after a few days, while surrounding waters
101 showed high chlorophyll *a* values until December 2020 (Supplementary Fig.
102 S8). Starting from January, the chlorophyll *a* concentration inside Eddy 2 was
103 similar to the surrounding region, but lower than inside Eddy 1 (Eddy 1: \sim
104 0.17 mg/m³; Eddy 2: ~ 0.10 mg/m³).

105 To include (maybe): Primary productivity (Time series)

106 2.2 Detailed eddy analysis based on float data

107 2.2.1 Temperature, Mixed Layer, Brunt-Väisälä frequency

108 Conservative temperature (hereafter temperature), obtained from in situ tem-
109 perature (Methods), was used to calculate the mixed layer depth (defined) as
110 the depth at which the temperature changed by 0.2° compared to the temper-
111 ature at 10 m depth, ref. [1] and Subsec. 4.3). This was about 65 m at the
112 beginning of the float deployment and started to deepen at the end of May to a
113 maximum depth of about 181 m on the 13 August just after the merging event
114 (Fig. 2b). Subsequently, it shoaled again to ~ 106 m depth on the 23 September
115 when the float left the eddy. The Brunt-Väisälä frequency - an indicator of
116 water column stability - above the mixed layer was mostly lower than $1.5 \cdot 10^{-6}$
117 s⁻² (Supplementary Fig. S9), supporting the view that the surface layer was
118 well mixed. Strong stratification, with Brunt-Väisälä frequency values around
119 $1.5 \cdot 10^{-4}$ s⁻², were observed about 50 m below the mixed layer depth. This
120 suggested that the eddy core (defined as the layer between the 1026.80-1027.24
121 kg/m³ isopycnals and corresponding to ~ 200 -600 m depth) was well isolated
122 from the surface waters. Intermediate Brunt-Väisälä frequency values ($9.1 \cdot 10^{-6}$
123 s⁻²) suggest intermediate internal mixing within the eddy core. Temperature in
124 the mixed layer steadily decreased during the entire study period, from about
125 20.7°C to 15.2°C, likely due to mixing in of colder waters from below and the
126 decline in solar radiation in Austral Winter. Temperature in the eddy core was
127 constant from the 20 April to the eddy merging event ($\sim 6.87^\circ$). Subsequently,
128 it decreased to 6.74° when the float left the eddy. The temperature anomaly
129 in the mixed layer was positive until July (Supplementary Figure S5). It then
130 became negative in the upper 50 m of the water column and positive beneath.

154 2.2.2 Oxygen

155 The dissolved oxygen concentration in the mixed layer steadily increased from
156 228 to 248 $\mu\text{mol}/\text{kg}$, likely due to the concomitant temperature decrease (Fig.
157 2c and Supplementary Fig. S2b). The dissolved oxygen concentration in the

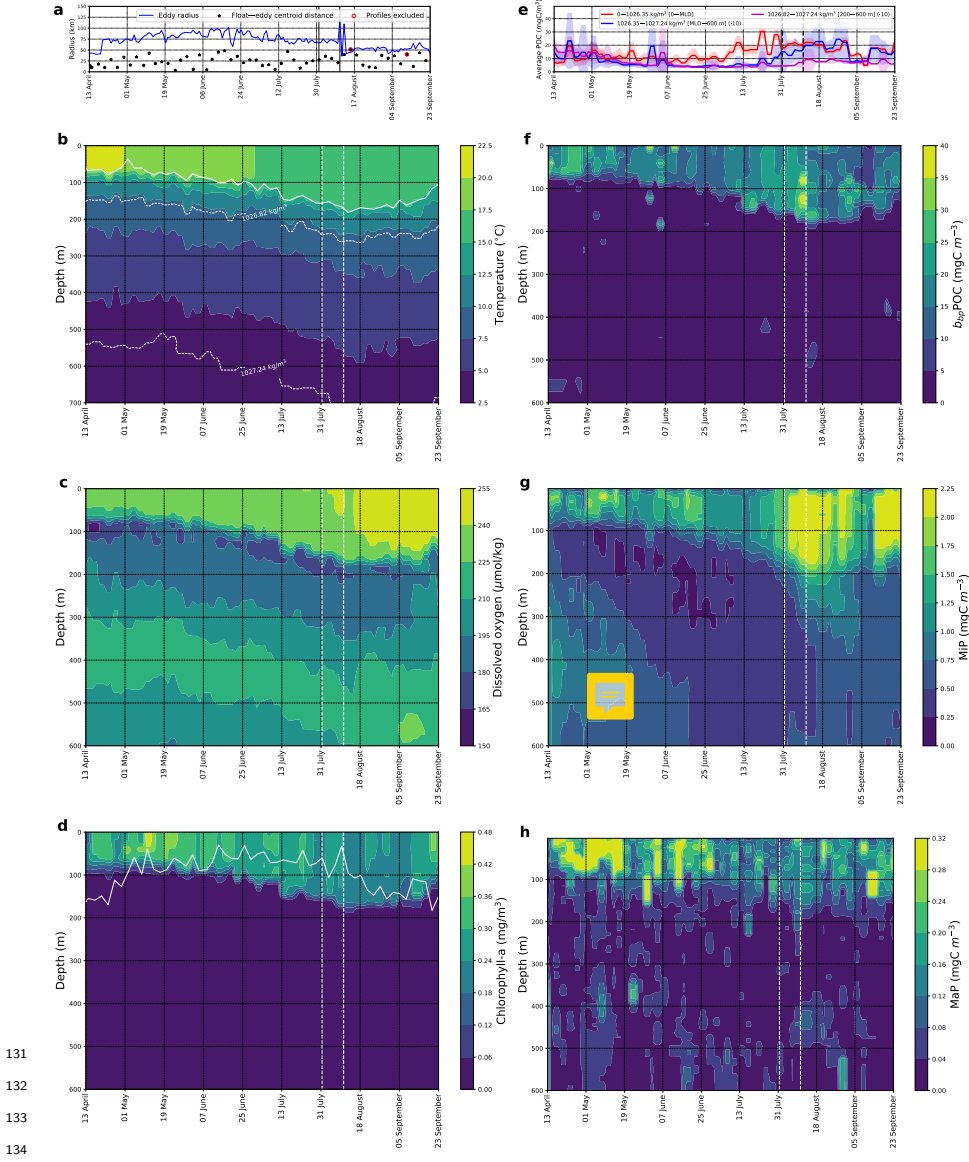


Figure 2: Panel **a**: Time series of the eddy radius (blue solid line) and the distance of the float from the eddy center (black stars). Panels **b–d**: conservative temperature (panel **b**), dissolved oxygen (**c**), and chlorophyll *a* (**d**) as a function of time and depth. Panel **e**: Time series of the average POC (calculated as the sum of the particulate backscattering b_{bp} , MiP and MaP POC) integrated between the surface and the mixed layer depth, shown as a red solid line. The average POC in the eddy core (comprised between the 1026.82–1027.24 kg/m³ isopycnals, white dashed lines in panel **b**) and between the mixed layer and the eddy core lower limit are shown as magenta and blue solid lines, respectively.

145 Figure 2: (on previous page) Both are ten-fold magnified to improve visibility.
146 Uncertainties (standard deviation) are reported as shadowed regions. Panels
147 **f–h**: b_{bp} (**f**), MiP (**g**), and MaP (**h**) POC as a function of time and depth. The
148 vertical dashed lines (colored in black in panels **a** and **e**, in white in panels **b–d**
149 and **f–h**) indicate, respectively, the beginning and the end of the merging event
150 between Eddy 1 and 2. The mixed layer and critical depths are showed as white
151 solid lines in panels **b** and **d**, respectively. Note that in panel **b**, temperature is
152 reported down to 700 m to show the eddy core.
153

158 eddy core slightly decreased between the 21 April and the 13 August from 208 to
159 200 $\mu\text{mol}/\text{kg}$ (Supplementary Fig. S3b). After the eddy merging, it increased to
160 more than 208 $\mu\text{mol}/\text{kg}$ on the 12 September. The Apparent Oxygen Utilisation
161 (AOU, defined as the difference between the theoretical oxygen concentration
162 at saturation levels and the measured dissolved oxygen) in the mixed layer was
163 slightly negative until the 20 June (-2.9 $\mu\text{mol}/\text{kg}$), indicating over-saturation,
164 and close to 2.0 $\mu\text{mol}/\text{kg}$ until the 9 September, when it became negative again
165 until the float left the eddy (Supplementary Figure S13).
166

167 2.2.3 Chl a

168 A peak of the mean chlorophyll *a* concentration in the mixed layer (0.44 mg/m³)
169 was observed on the 11 May 2021 (Fig. 2d, Supplementary Fig. S2c), which
170 might be related to oxygen production, thus possibly explaining the negative
171 AOU during that period. Subsequently, the chlorophyll *a* concentrations grad-
172 ually decreased until the 12 August (0.19 mg/m³), and started to increase again
173 after the 9 September. The depth down to which chlorophyll *a* could be found
174 closely followed the mixed layer depth. Between May 2021 and the merging
175 event, chlorophyll *a* integrated over the mixed layer steadily increased from 15
176 mg/m² to 43 mg/m² (Supplementary Fig. S2d). Subsequently, it did not change
177 significantly. The Sverdrup critical depth (Svcd; MM 4.1) is the depth at which
178 the integrated primary productivity and the algal respiration balance each other
179 ([2]). Suitable conditions for phytoplankton growth exist when the critical depth
180 is deeper than the mixed layer depth, and vice versa. In general, the Svcd fol-
181 lowed the seasonal trend of surface irradiance, becoming shallower until July
182 2021 (austral Winter) and then deepening again. The Svcd was deeper than the
183 mixed layer from Mid April to the beginning of May, thereafter both were more
184 or less equal until beginning of June, when the Svcd became shallower than the
185 mixed layer. Both depths were similar again in September 2021.
186

187 2.2.4 Particle stocks within the mixed layer and the eddy core

188 The average POC content within the mixed layer (calculated using a particulate
189 backscatter b_{bp} to carbon [3] and a UVP particle size to carbon relationship

(Methods and ref. [4]); particle size considered: 0.102 to 16.40 mm diameter) was rather constant between the 13 April and the 3 July (7.9 mgC/m^3 ; Fig. 2e). It then increased to 22.0 mgC/m^3 on the 10 July. During the eddy merging event, it slightly increased from 18.1 mgC/m^3 to 21.2 mgC/m^3 . The average POC content in the eddy core was found to be about 1.95 mgC/m^3 on the 13 April (Fig. 2e). It then gradually decreased until the end of June (except for a peak on the 5 June). Subsequently, it started to increase on the 5 August (during the eddy merging event), reaching 0.92 mgC/m^3 on the 12 August. The average POC content integrated between the 1026.35 kg/m^3 isopycnal (which closely followed the mixed layer depth, Supplementary Fig. xx) and the lower boundary of the eddy core (i.e., the 1027.24 kg/m^3 isopycnal) showed a similar trend, with a more intense POC increase between the 21 July and the 26 August, reaching 2.45 mgC/m^3 .

The POC content calculated from b_{bp} data is considered as representative of particles between 0.001–0.025 mm [5]. Within this small size class we see that the b_{bp} POC in the mixed layer decreased from 18.5 mgC/m^3 in April to 12.3 mgC/m^3 on the 25 June, it then increased to 24.5 mgC/m^3 on the 7 August (during the eddy merging event) and decreased afterwards (Fig. 2f and Supplementary Fig. S2e). The b_{bp} POC concentration in the eddy core showed consistently lower values, with 1.05 mgC/m^3 on average in April which decreased to 0.24 mgC/m^3 between July and September. Notably, the b_{bp} POC concentration peaked to 0.65 mgC/m^3 on the 12 August, just after the eddy merging event, and decreased afterwards.

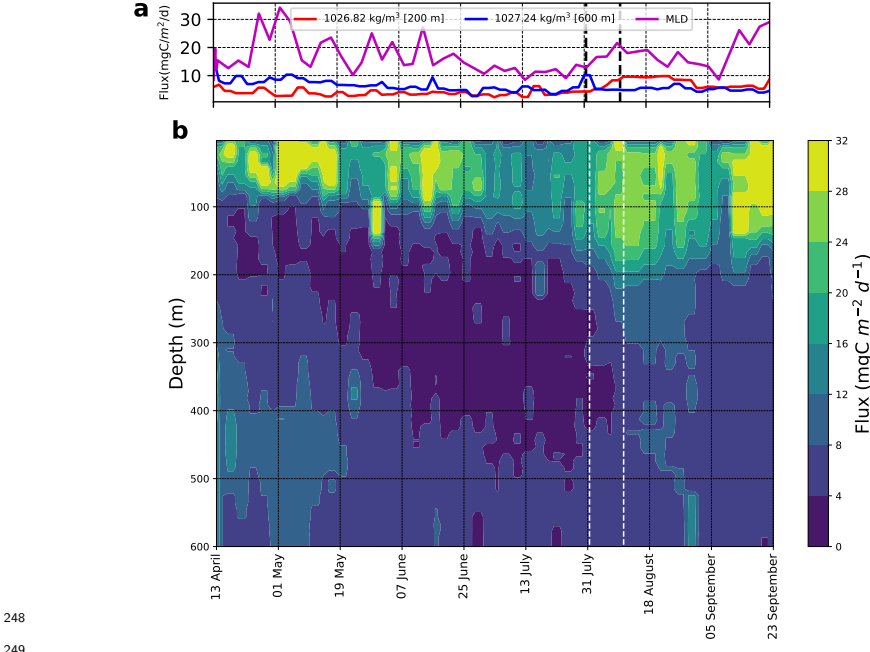
Micrometric particle (MiP; particle with 0.12 to 0.51 mm diameter) POC concentration within the mixed layer (Fig. 2g, Supplementary Fig. S2f) increased from 0.65 mgC/m^3 in April–July to more than 2.19 mgC/m^3 during the eddy merging event in August. A layer of increased MiP concentration was present in the eddy core at the float release. This layer was characterised by a MiP POC concentration of 0.93 mgC/m^3 which gradually decreased to 0.31 mgC/m^3 on the 26 June. It then increased prior and after the eddy merging event up to 0.77 mgC/m^3 until the 25 August.

Macroscopic particle (MaP; particle with 0.51 to 16.40 mm diameter) POC concentration (Fig. 2h, Supplementary Fig. S2g) in the mixed layer was above 0.28 mgC/m^3 during April and May 2021. Subsequently, it decreased below 0.13 mgC/m^3 in July and August, and did not change significantly during the eddy merging event. In the eddy core, MaP POC showed low values over the whole time period ($0.03 \pm 0.01 \text{ mgC/m}^3$), slightly decreasing in April and then being constant.

add a figure with ML and 1026.35 kg/m^3 isopycnal to show they are very similar

2.2.5 Carbon flux dynamics

POC flux was calculated by integrating the POC fluxes of each size class between 0.102–16.40 mm. The latter were obtained assuming the POC concentration and the sinking speed of each size class (Methods). The size–sinking speed relationship proposed by Kriest et al. [4] (ref. 9 in their Table 2) was used. The



248
249
250 Figure 3: Panel a: Time series of POC flux along the 1026.35 kg/m^3 isopycnal
251 and the mixed layer depth (magenta solid and dashed lines, respectively). The
252 red and blue solid lines show the time series of POC flux along the 1026.8
253 and 1027.2 kg/m^3 isopycnals, which delimit the eddy core and are located at an
254 average depth of 200 and 600 m, respectively. Panel b: POC flux as a function of
255 time and depth. In both panels, the vertical dashed lines indicate, respectively,
256 the beginning and the end of the merging event between Eddy 1 and 2.

234 flux values measured in the present study were in agreement with independent
235 flux observations carried out in the same region (Supplementary Fig. S10).
236 The POC flux at the lower boundary of the eddy core was larger than the POC
237 flux at the upper boundary between the 13 April and the 3 August, ($6.63 \text{ vs } 3.82$
238 $\text{mgC m}^{-2} \text{ d}^{-1}$, respectively; Fig. 3a). During the eddy merging event, the flux
239 at the upper boundary of the eddy core increased, reaching $9.60 \text{ mgC m}^{-2} \text{ d}^{-1}$
240 on the 12 August. The same trend was observed in the flux at the mixed layer
241 depth, which reached 21.59 mgC m^{-2} on the 10 August. The presence of a layer
242 of increased POC flux in the eddy core was visible when the float was released
243 (Fig. 3b and Supplementary Fig. S3f, $21.59 \text{ mgC m}^{-2} \text{ d}^{-1}$) and then gradually
244 decreased until the 23 July ($3.27 \text{ mgC m}^{-2} \text{ d}^{-1}$). Subsequently, the POC flux
245 in the eddy core increased up to $8.16 \text{ mgC m}^{-2} \text{ d}^{-1}$ on the 30 August. MiP
246 mainly contributed to the POC flux both at upper boundary of the eddy core
247 (71% of the total POC flux) and at its lower boundary (87%).

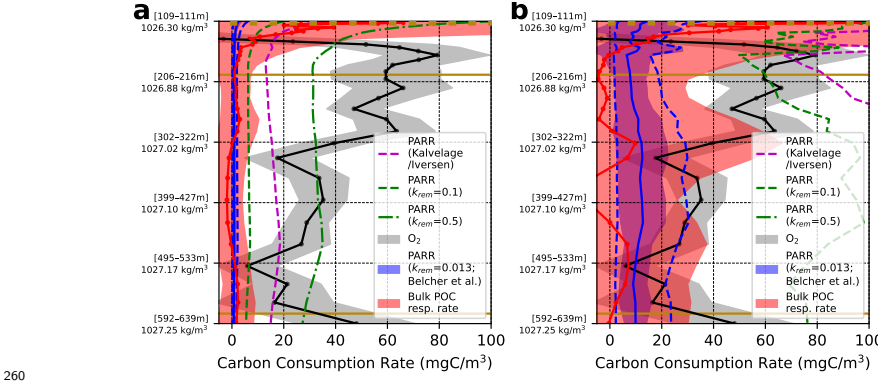
258 **2.3 Mesopelagic carbon supply and oxygen demand prior
259 to eddy merging**

282 Here, we analyse the carbon and oxygen dynamics between the mixed layer
283 depth down to lower boundary of the eddy core. We only consider the time
284 window prior to the eddy merging (13 April–31 July) when the water column
285 was relatively well isolated. Thus, we consider that the float tracked the same
286 water mass in a quasi-Lagrangian way. Particle-Associated Respiration Rate
287 (PARR) was calculated by combining the particle size, the POC content, and
288 specific carbon remineralization rate (k_{rem} , ref. [6] and Methods) and by inte-
289 grating over the 0.102–16.40 mm size classes.

290 To calculate the *bulk POC respiration rate* (Methods 4.3) we consider a layer
291 between two isopycnals. The difference between the POC flux entering and ~~the~~
292 ~~POC flux~~ exiting this layer can be considered as the carbon flux supply; the
293 difference between the integrated POC at the beginning and at the end of the
294 time period represents the carbon stock change in the layer. The *bulk POC*
295 *respiration rate* then is the difference between the carbon flux supply and the
296 change in the carbon stock. We find that on average 1.12 mgC/m^3 entered
297 the eddy core at its upper boundary and 2.00 mgC/m^3 left at its lower bound-
298 ary, resulting in a negative flux difference of $-0.88 \pm 0.69 \text{ mgC/m}^3$ before the
299 eddy merging event. The carbon stock decreased by $1.41 \pm 1.18 \text{ mgC/m}^3$, hence
300 we estimate a bulk POC respiration rate of $0.53 \pm 1.36 \text{ mgC/m}^3$ for the eddy
301 core. We can now compare this value with estimates of PARR assuming dif-
302 ferent k_{rem} , which are converted to carbon remineralization rate of 0.88 ± 0.37
303 mgC/m^3 assuming a respiratory quotient of 0.89 molC/molO_2 . The bulk POC
304 respiration rate was calculated for the layer between 1026.30 – 1026.35 kg/m^3
305 isopycnals. This was repeated until the 1027.20 – 1027.25 kg/m^3 isopycnal layer
306 (Fig. 4). We find that a k_{rem} of 0.013 d^{-1} [6] yields the best match between
307 the bulk POC respiration rate and PARR : bulk POC respiration rates ranged
308 between $-1.93 \pm 5.83 \text{ mgC/m}^3$ and $3.02 \pm 7.34 \text{ mgC/m}^3$, while PARR ranged be-
309 tween $0.56 \pm 0.03 \text{ mgC/m}^3$ and $0.91 \pm 0.29 \text{ mgC/m}^3$. PARRs calculated with
310 greater remineralization rates k_{rem} (0.1 and 0.5 d^{-1}) are larger than the bulk
311 POC respiration rates.

312 The bulk POC respiration rate and the PARR can also be compared with the
313 oxygen consumption rate, derived as the change of oxygen within the layer be-
314 between two isopycnals. This can be converted to a carbon consumption rate using
315 a respiratory quotient of 0.89 molC/molO_2 (Methods) and thereby serve as an
316 independent metric to constrain our bulk POC respiration rates (Fig. 4a). Oxygen
317 consumption rate ranged between 44.1 – 77.2 mgC/m^3 along 1026.825 – 1027.025
318 kg/m^3 isopycnals (175 – 195 m depth), and then decreased to 5.0 – 30.1 mgC/m^3
319 along 1027.05 – 1027.10 kg/m^3 isopycnals (320 – 365 m depth). It then reached
320 41.2 – 41.2 mgC/m^3 along 1027.10 – 1027.175 kg/m^3 isopycnals (373 – 484 m depth),
321 and -1.2 – 30.3 mgC/m^3 along 1027.20 – 1027.25 kg/m^3 isopycnals (520 – 581 m
322 depth). Below, it showed spiky values, likely due to the poor isolation of wa-
323 ters below the eddy core. In general, bulk POC respiration rate estimates and
324 PARR were 10 – 20 times lower than the oxygen consumption rate, except be-

provide references, or
delete the ones we
don't have
...



260
 261 Figure 4: Panel **a**: Bulk POC respiration rate in the water column (red line)
 262 calculated from the difference of the POC influx (the POC flux entering from
 263 above minus the POC flux exiting from the bottom) and the integrated POC
 264 (sum of MaP, MiP, and b_{bp} POC) variation between the 4 April and the 31 July
 265 2021 (Methods). Each red dot represents the bulk POC respiration rate ob-
 266 tained for the layer comprised between two isopycnals separated by 0.05 kg/m^3
 267 (from $1026.30\text{--}1026.35 \text{ kg/m}^3$ to $1027.25\text{--}1027.30 \text{ kg/m}^3$). The mean depth of
 268 the isopycnal layer studied is indicated by the values within brackets on the
 269 y -axis. The red shadowed area represents the uncertainty (standard deviation,
 270 MM). The blue line shows the PARR calculated with $k_{rem}=0.013 \text{ d}^{-1}$, while
 271 the blue area delimits the PARR values obtained with k_{rem} between $0.003\text{--}0.031$
 272 d^{-1} [6]. The green dashed lines show the PARR obtained with $k_{rem}=0.1\text{--}0.5$
 273 d^{-1} . The magenta dashed line shows the PARR obtained with the formulation
 274 by Kalvelage et al. Panel **b**: same as panel **a**, with the difference that the bulk
 275 POC respiration rate and the PARR metrics were calculated considering also
 276 the size classes between $0.025\text{--}0.1 \text{ mm}$. In both panels, the black lines represent
 277 the oxygen consumption rate, and the shadowed gray area shows the associated
 278 uncertainty (standard deviation on the regression slope, MM for details). The
 279 golden solid lines show the upper and lower limits of the eddy core, while the
 280 golden dotted line shows the mixed layer depth.

325 tween 520–581 m depth (layer along ~ 1027.17 – 1027.24 kg/m³ isopycnals).
326 Between the mixed layer depth and the upper boundary of the eddy core, bulk
327 POC respiration rate was associated with large uncertainties, possibly due to
328 the poor isolation of the water mass within this layer; the oxygen consumption
329 rate became negative, likely due to the production of oxygen and the potential
330 mixing of waters from the mixed layer.
331 To further explore this question, we recalculated the bulk POC respiration
332 rate and the PARR including the smallest size class concentrations (between
333 0.025–0.1 mm). These were extrapolated from the particle size abundance (MM
334 4.3) and their POC content was consistent with the b_{bp} POC concentration (Sup-
335 plementary Fig. S11), considered as representative of particles between 0.001–0
336 0.025 mm [5]. Both the bulk POC respiration rate and the PARR increased by
337 one order of magnitude and were consistent with the oxygen consumption rate
338 between 1027.02–1027.24 kg/m³ isopycnals (310–600 m; Fig. 4b). However, the
339 associated uncertainties increased as well, and bulk POC respiration rate showed
340 negative values (-8.1 ± 38.4 mgC/m³) along 1027.10–1027.125 kg/m³ isopycnals.
341 All the metrics were calculated reducing the length of the time period down to
342 the 20 June, obtaining consistent trends (Supplementary Fig. xx).

3 Discussion

343 Removed discussion sections from results and pasted below, no order yet!!!

344 Discuss why eddy subducted, what are the driving processes causing this

345 Mention in discussion that eddy was stable and large, this why we chose it
346 (((+ that cyclones are less studied / targeted??)))

347 Remi's comment: What can be said, however, is that cyclones are less in-
348 tense and more likely to disappear quickly and thus more "difficult/risky" to
target.

349 Rainer comment: need to mention the fact that the increase in POC in the
350 0–200m layer does not necessarily mean that production increased, but can
351 be due to algal organisms in aggregates that therefore became more visible

352 Mention that flux at upper eddy core boundary was smaller than the flux at
353 the eddy core lower boundary until the eddy merging, which is not what one
354 would expect

355 First, even if upwelling eddies are expected to trap nutrient-rich upwelled
356 waters and propagate westward, there are few cases that provide such evidence
357 (Schütte et al., 2016b; Karstensen et al., 2017) and it happens to be mostly
358 anticyclonic cases. So this cyclone is really a unique case where we have both
biological and hydrographic temporal information combined.

359 At a global level, Argo floats that were trapped in cyclones are on average
360 significantly less than those trapped in anticyclones (Gaube et al. 2019).

361 On the other hand, the Cape Basin is an area well known for Agulhas Rings
362 that provide a significant intrusion of warm/salty waters (Remis work) and it is

359 mostly populated by cyclones which mainly originate from the upwelling shelf
360 (Boebel et al. 2003). So it is really an important upwelling cyclone example!

361 Different considerations suggest that the BGC Argo float targeted the same
362 water mass during the time period of interest: the distance of the float from the
363 eddy center was always lower than the eddy radius (Fig. 2a); the 200–600 m
364 water column showed a consistent temperature anomaly during the whole period
365 studied (Supplementary Fig. S5); third, the mixed layer was well above 200 m
366 and Brunt-Väisälä frequency showed intermediate values in the 200–600 m water
367 column, suggesting a limited mixing of water from above ; furthermore, the
368 chlorophyll *a* signature showed that the eddy was isolated from the surrounding
369 waters (Subsec. 2.2 and Supplementary Fig. S8).

370 We analysed the 200–600 m water column between the 13 April and the
371 31 July 2021. The dissolved oxygen and MiP POC concentrations steadily de-
372 creased during that time period, while b_{bp} POC showed constantly low values,
373 further corroborating the view that these waters were relatively well isolated
374 during that period. Furthermore, the lack of a b_{bp} POC scattering signal sug-
375 gests that this structure did not originate from coastal waters, as these are rich
376 of micrometric particles which would have been detected with the b_{bp} . Also,
377 the relatively low chlorophyll concentration in the months preceding the BGC
378 Argo deployment suggested that these particles were not from the settling of
379 a previous productivity events. However, satellite-derived chlorophyll *a* maps
380 may miss deep chlorophyll *a* maximum, not allowing us to exclude this hypoth-
381 esis. A further explanation would be the trapping of a cloud of relatively old
382 particles during the formation of the eddy, which were retained in the following
383 months.

384 In recent years, approaches have been developed to calculate particle-associated
385 respiration rates (PARR) from UVP5 particle size distribution data (Kalvelage
386 et al., Bianchi et al), based on laboratory measurements of individual particle
387 respiration rates [7]. However, so far it was impossible to test the validity of
388 these approaches *in situ* as it was not possible to measure bulk POC respi-
389 ration rates. Our results showed a consistent agreement between PARR and bulk
390 POC respiration rates, suggesting that a remineralization rate of 0.013 d^{-1} best
391 represents the carbon remineralization rate at 200 to 600 m depth in our study
392 region. The mismatch between PARR and bulk POC respiration rates with
393 oxygen consumption rates indicated that the oxygen consumption could not be
394 uniquely due to the respiration associated with POC particles in the size range
395 $0.102\text{--}16.40 \text{ mm}$.

396 The best consistency (obtained when extending particle spectra) between the
397 bulk POC respiration rate, the PARR, and the oxygen consumption rate (Fig.
398 4a versus Fig. 4c) as well as a better match with independent POC flux measure-
399 ments (Supplementary Figure S10) suggested that the majority of respiration
400 occurred within particles smaller than 0.1 mm. This is in agreement with recent
401 studies indicating that small particles are quickly remineralized REF. However,
402 our findings suggest that these particles should be abundant and thus contribute
403 importantly to the POC budget, which is in contrast with previous considera-
404 tions ([8]).

405 The gap between the oxygen consumption and the POC respiration in the
406 250–350 m layer could be due to the DOC consumption at those depths, even
407 if we could not observe it directly. Interestingly, DOC consumption rates have
408 been reported in the order of xx mgC/m² at 200 m depth, decreasing to 0 at
409 400 m REF. These values are consistent with the gap observed between oxy-
410 gen consumption and POC respiration, and with its trend that decreases with
411 depth. DOC presence in the eddy may be explained by the intense chlorophyll
412 *a* concentration inside the eddy, especially at its early stages (Supplementary
413 Figure S8).

414 When comparing the quiescent and the flux event periods in the mesopelagic, the
415 oxygen consumption increased, while the PARR remained stable (Fig. 4). This
416 suggested that the remineralization at depth was mainly driven by small parti-
417 cles not detected by the UVP6, and potentially coming from the fragmentation
418 of larger exported particles. The 20 June 2021 was chosen as date separating
419 the quiescent and flux event periods because it showed the best results in terms
420 of agreement between bulk POC respiration rate, PARR, and oxygen consump-
421 tion rate. This was likely due to the export event starting in the middle of
422 July 2021, which hampered the isolation of the water column, affecting both
423 oxygen and respiration rates. However, when changing the separating date, we
424 obtained consistent agreements between these metrics as well.

425 Despite the presence of an inverse trend between MiP and MaP in the
426 epipelagic, it was unlikely that MaP particles were broken in MiP particles.
427 This because the MiP increase and Map decrease occurred months apart, and
428 shifts in the ecosystems observed are likely to occur (REF).

429 The flux event was visible in the POC flux and in the average MiP POC
430 concentration in time (Fig. 2e, Fig. 3a,b).

431 In the weeks preceding the flux event, the critical depth was well above the
432 mixed layer depth (Fig. 2c). Indeed, the chlorophyll *a* concentration started de-
433 creasing in the beginning of June 2021, when the critical depth became shallower
434 than the mixed layer depth. This indicated the absence of favourable conditions
435 for the phytoplanktonic organisms during that time window, possibly triggering
436 the flux event.

437 This increase might have been triggered by a shoaling of the critical depth,
438 leading to unfavourable conditions for phytoplankton growth.

439 The relationship between the particle size and its sinking speed was based
440 on an empirical relationship obtained by Kriest et al. [4], and which was in
441 agreement with the sinking speeds obtained from our time series (Supplementary
442 Fig. ??). The sinking speeds obtained are lower compared to the values reported
443 in other studies for other regions. This can be due to the peculiar characteristics
444 of our case study, and to the fact that a rigorous validation of size–sinking speed
445 relationships is still lacking and it is a matter of debate [7]. When using a
446 different relationship (implying larger sinking speeds, Supplementary Fig. ??),
447 the bulk POC respiration rate, PARR, and oxygen consumption showed a good
448 agreement (Supplementary Fig. ??).

449 **4 Materials and Methods**

450 **4.1 Satellite data**

451 **Absolute dynamic topography**

452 Absolute dynamic topography (ADT) was downloaded from the Copernicus Ma-
453 rine Environment Monitoring Service (CMEMS, <http://marine.copernicus.eu/>).
454 This represented the sum of the sea level anomaly and the mean dynamic topog-
455 raphy, was derived from 12 altimetric missions, and produced by Ssalto/Duacs
456 at 0.25° spatial resolution and one day of temporal resolution [9].

457 **Sea surface chlorophyll**

458 Estimations of chlorophyll *a* concentration in the region of interest were obtained
459 from the Global Ocean Color product (OCEANCOLOUR_GLO_CHL_L4 REP_OBSERVATIONS_009_082-
460 TDS) produced by ACRI-ST. This was downloaded from CMEMS website. The
461 spatial resolution of the product is 1/24° and the temporal resolution is one day.

462 **Sverdrup critical depth calculation**

463 Sverdrup critical depth Z_c was calculated for each profile using the formulation
464 of Kováč et al. [10]:

$$Z_c = \frac{1}{K} \left[W\left(-\frac{\alpha^B I_T}{L_T^B} \exp\left(\frac{-\alpha^B I_T}{L_T^B}\right)\right) + \frac{\alpha^B I_T}{L_T^B} \right], \quad (1)$$

465 where K is the attenuation coefficient, W is the Lambert function, i.e.
466 the solution of the generic equation $xe^x = a$, α^B is the initial slope of the
467 photosynthesis-irradiance function [11], I_T the total available light energy at
468 the surface over one day, and L_T^B the phytoplankton loss rate. As K , we used
469 the Downwelling Diffuse Attenuation Coefficient Data at 490 nm and 8-day
470 temporal resolution (to improve coverage and reduce missing data) downloaded
471 from Nasa Ocean color website (<https://oceandata.sci.gsfc.nasa.gov>, [12]). For
472 each profile, K was calculated as the mean attenuation coefficient in a circu-
473 lar neighborhood of radius 0.1°, centered on the profile location, to smooth
474 errors. As α^B we used the mean of 25 measures obtained in our study region
475 ($0.118 \pm 0.061 (mgC/mgChla/h)/(W/m^2)$, [11]). To obtain I_T we multiplied the
476 day length at each profile location by the surface irradiance I_0 . The latter was
477 the Daily Shortwave Solar Irradiance - MSG product, provided by Osi Saf con-
478 sortium at 0.05° and daily temporal resolution, and downloaded from Eumetsat
479 Data Center (<https://archive.eumetsat.int>). I_0 was calculated for each profile
480 location in a circular neighborhood of radius 0.1° in the same way as for K . As
481 L_T^B , we used a value of 1.75 mg C/mg Chl a/h obtained by [13].

482 **4.2 Eddy detection**

483 **TOEddies algorithm**

484 Remi, Artemis, Sabrina

485 **Chlorophyll *a* anomaly calculation**

486 Once the eddy centers and contours were identified, we defined the chlorophyll
487 *a* anomaly as the difference between the mean chlorophyll concentration inside
488 the eddy and the region surrounding it. The former was extracted from the
489 mean chlorophyll *a* concentration inside the maximal velocity eddy contour.
490 The latter was extracted from the mean chlorophyll *a* concentration inside a
491 circular neighborhood centered on the eddy center, with radius equal to ~ 340
492 km, minus the region inside the maximal velocity eddy contour. The radius was
493 set to ~ 340 km, corresponding to 4 times the mean eddy radius calculated with
494 the outermost contour (~ 85 km), to have a proper representation of the region
495 in which the eddy was located.

496 **4.3 BGC Argo data**

497 **Argo deployment**

498 How eddy was chosen? Within the eddy, how the deployment location was
499 chosen?

500 **Validation of Argo measurements**

501 (description of processing from adjusted to delayed time)

502 **UVP6 description?**

503 **Mixed layer depth calculation**

504 Mixed layer depth was calculated as the depth at which the temperature de-
505 creased of 0.2° compared to the temperature at 10m depth, following the defi-
506 nition of d'Ortenzio et al. [1]

507 **Temperature anomaly calculation**

508 Remi or Artemis could you please check the following sentences?

509 Temperature anomaly was calculated by subtracting the temperature mea-
510 sured by the float to the temperature climatology obtained from the World
511 Ocean Atlas (WOA; <https://www.ncei.noaa.gov/products/world-ocean-atlas>) for
512 the years yyyy-yyyy

513 **Depth and density calculation, filtering and interpolation of variables**
514 **in depth and time**

515 Depth, mixed layer depth, conservative temperature, absolute salinity, and sea-
516 water density were calculated from the Gibbs SeaWater Oceanographic Toolbox
517 of the Thermodynamic Equation of SeaWater [14]. For a given parameter, we
518 applied, for each BGC Argo profile, a Savitzky–Golay filter (Python module
519 scipy) to smooth the spikes while keeping signal consistency. Subsequently, we
520 interpolated the filtered profiles in time and depth with a resolution of one day
521 and 10 meters using the grid data function from the Python module scipy.

522 **Particulate Organic Carbon concentration and flux calculation**

523 High-resolution full-depth particle size abundances (expressed as number of par-
524 ticles per liter; #/L) were obtained with an Underwater Vision Profiler 6 [15].
525 The size classes ranged between 0.102 and 16.40 mm of equivalent spherical
526 diameter (ESD). Particulate Organic Carbon (POC) concentration for a given
527 size class was obtained by multiplying its particle abundance and the relative
528 POC content. The latter was obtained from the empirical relationship between
529 particle size and nitrogen content measured in ref. [4] (reference 2a in their
530 Table 1) and assuming a carbon:nitrogen ratio of 106:16.

531 Micrometric particles (MiP) POC concentration was obtained by integrating
532 the POC concentrations over all size classes between 0.1–0.5 mm. Macroscopic
533 particle (MaP) POC concentration was calculated analogously using the size
534 classes between 0.5–16 mm.

535 Particulate backscattering (b_{bp}) was considered representative of particles be-
536 tween 0.001–0.030 mm and was converted to b_{bp} POC concentration using the
537 relationship of [3], adopted in several studies (e.g. [16, 17]).

538 Average POC concentration in the 0–200 and 200–600 m layers was obtained
539 from the mean value of the sum of MiP, MaP, and b_{bp} POC concentrations in
540 these layers.

541 POC flux for a given size class was calculated using its POC concentration and
542 assuming the empirical relationship between particle size and sinking speed of
543 ref. [4] (ref. 9 in their Table 2). This relationship best reproduced profiles of
544 marine snow and particulate aggregates at the same time, and has been adopted
545 in previous studies using UVP observations (e.g. [18]). This lead to a POC flux
546 ($\text{mgC m}^{-2} \text{ d}^{-1}$) = $1.4324 \text{ ESD}^{2.24}$, with ESD in cm. Finally, the total POC
547 flux was obtained by integrating over the size classes between 0.1–16 mm.

548 POC flux, MiP, MaP, and b_{bp} POC were filtered and interpolated in depth and
549 time following the same procedure described in the previous Subsection for tem-
550 perature, salinity, etc.

551 **Particle-Associated Respiration Rate calculation**

552 Particle-Associated Respiration Rate (PARR) for a given size class was calcu-
553 lated using two different functions:

- 554 • the first function combined the size class ESD, the POC concentration,
 555 and a specific carbon remineralization rate k_{rem} using ref. [6]. We used
 556 $k_{rem}=0.013 \text{ d}^{-1}$, which was measured empirically by [6] on marine snow
 557 aggregates in the Atlantic Ocean. To calculate the associated uncertainty,
 558 we used the k_{rem} values of 0.003 and 0.031 d^{-1} provided by [6]. Finally,
 559 we included the temperature (T) effect by dividing the values obtained
 560 by $3.5^{(10-T)/10}$. k_{rem} values of 0.100 and 0.500 d^{-1} were used as well [7]
 561 REF.

 562 • the second function combined the size class ESD, the POC concentra-
 563 tion, the temperature, and the oxygen concentration, and was obtained
 564 by Kalvelage et al. The PARR obtained in this way gave the same results
 565 than the PARR obtained with the function of ref. [7]. This because the
 566 study of Kalvelage et al. was based on the function from ref. [7] plus a
 567 correction for low oxygen conditions, which however did not apply in our
 568 study region (Fig. 2E).

569 Finally, the total PARR was obtained by integrating over the size classes be-
 570 tween 0.1–16 mm.

571 **Oxygen consumption rate calculation**

572 The oxygen consumption rate as a function of the depth was calculated as fol-
 573 lows. First, we selected a given isopycnal bin (e.g. 1026.80–1026.85 kg/m³).
 574 Then, for a given profile, we calculated the oxygen in correspondence with the
 575 selected bin as the mean of all the oxygen values measured within the bin range.
 576 This was repeated for all the profiles between the 23 April and the 31 July 2021,
 577 resulting in CHECK 28 oxygen values. These were linearly interpolated using
 578 the lin regress function from the Python module scipy, providing the oxygen
 579 consumption rate (the slope of the linear fit) with the associated uncertainty
 580 (the slope standard deviation). The depth associated with the isopycnal bin was
 581 calculated as the mean of all the depth values measured within the isopycnal
 582 bin during the period of time considered. This was repeated for all the isopy-
 583 cnal bins included between 1026.325 and 1027.40 kg/m³, providing the oxygen
 584 consumption rate at different depths. The choice of calculating the oxygen vari-
 585 ation along a given isopycnal value was to follow the same water mass over time.
 586 The oxygen consumption rate was converted to carbon consumption rate using
 587 a respiratory quotient of 0.89, which was obtained for planktonic material (del
 588 Giorgio and Williams, 2005).

589 **Bulk POC respiration rate**

590 The bulk POC respiration rate in the water column between the 4 April and
 591 the 31 July 2021 was calculated as follows. First, we selected a starting depth of
 592 200 m. The final depth was set 100 m deeper, i.e. to 300 m. The POC budget
 593 was obtained from the difference of two terms:

- 594 • Δ Flux: the difference between the POC flux at 200 m and at 300 m.
 595 The POC flux at 200 m (300 m) was obtained as follows. The POC flux
 596 was filtered and interpolated in space and time (see previous Subsection),
 597 obtaining one interpolated profile per day. For each interpolated profile,
 598 the flux at 200 m (300 m) was calculated as the mean of the flux values
 599 comprised between 185–215 m (285–315 m), i.e. using a depth bin of 30 m
 600 centered on 200 m (300 m) depth. This resulted in CHECK 68 values, one
 601 per each day between the 4 April and the 31 July 2021. The flux at 200 m
 602 (300 m) was obtained from the sum of the 68 values, and its uncertainty
 603 from the standard deviation.

 604 • Δ Integrated POC: the difference between the integrated POC on the 31
 605 July and that on the 4 April 2021. The integrated POC and its uncer-
 606 tainty on the 31 July (4 April) was obtained from the mean and standard
 607 deviation values of the sum of MiP, MaP and b_{bp} POC between 200 and
 608 300 m depth on the 31 July (4 April), multiplied by the layer thickness
 609 (i.e. 100 m).

610 This was repeated increasing the starting depth of 25 m until the 500–600 m
 611 layer was reached, providing the bulk POC respiration rate at different depths.
 612 The uncertainty on the bulk POC respiration rate was obtained by propagating
 613 the uncertainties on Δ Flux and Δ Integrated POC.

614 **Extrapolation to size classes <0.1 mm**

615 For a given profile, the slope of the particle size distribution (PSD) at a given
 616 depth was obtained using the particle concentrations and the size classes be-
 617 tween 0.1–16 mm, both log-transformed (lin regress function of Python module
 618 `scipy`). When the regression was significant (99.2% of the cases analysed), the
 619 relationship was used to calculate the particle abundance of the size classes be-
 620 tween 0.025–0.1 mm. 0.025 was fixed as lower limit as the b_{bp} was considered
 621 representative of smaller particles (between 0.001–0.025 mm, ref. [5]). The
 622 particle abundance was used to calculate the 0.025–0.1 mm size classes POC
 623 concentrations. The values found were generally consistent with the b_{bp} POC
 624 concentrations (Supplementary Figure S11). Therefore, the POC flux, the av-
 625 erage POC concentration, the PARR, and the bulk POC respiration rate were
 626 recalculated including the size classes between 0.025–0.1 mm. This improved the
 627 comparison between the POC flux we measured and independent observations
 628 in our study region (Supplementary Figure S10).

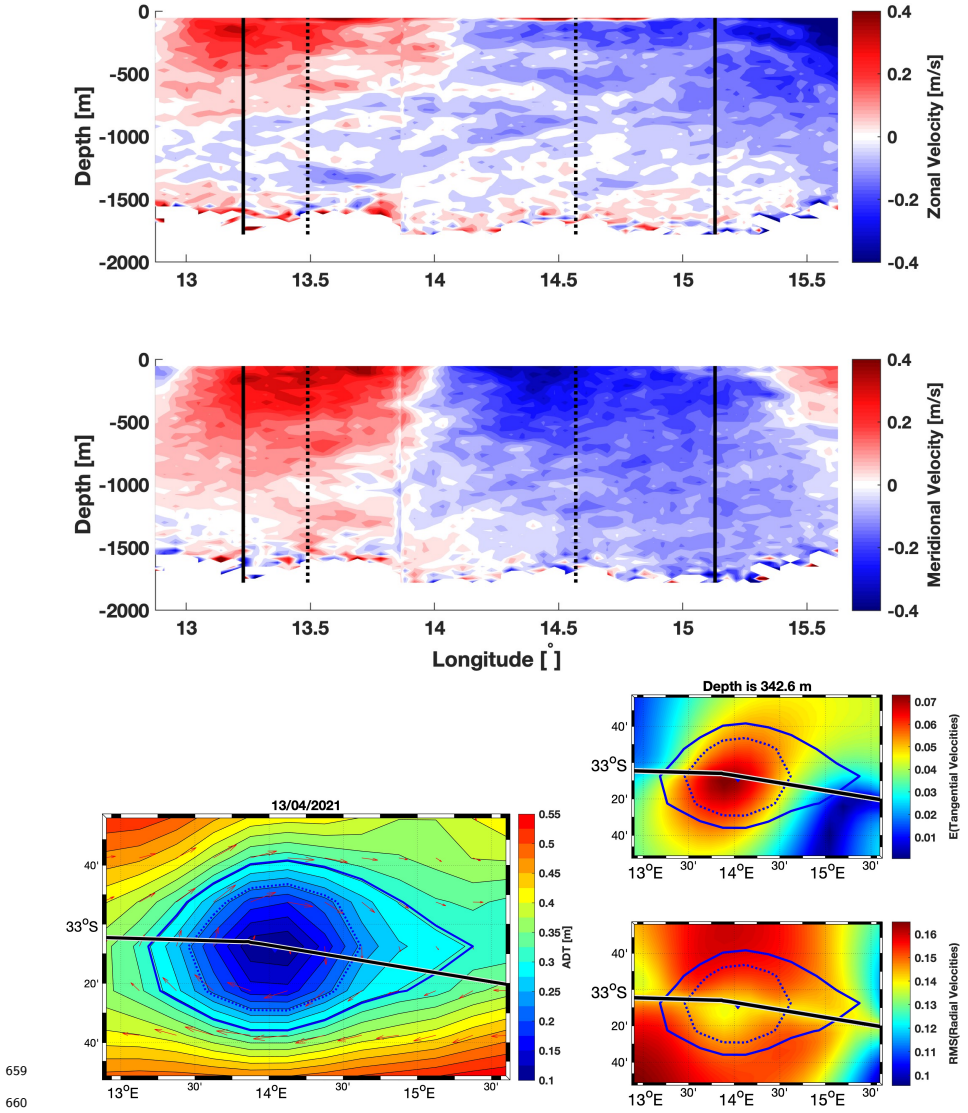
629 **References**

- 630 [1] F. D'Ortenzio, *et al.*, *Geophysical Research Letters* **32** (2005).
- 631 [2] H. Sverdrup, *Journal du Conseil* **18**, 287 (1953).
- 632 [3] I. Cetinić, *et al.*, *Journal of Geophysical Research: Oceans* **117** (2012).
- 633 [4] I. Kriest, *Deep Sea Research Part I: Oceanographic Research Papers* **49**,
634 2133 (2002).
- 635 [5] G. Dall'Olmo, T. K. Westberry, M. J. Behrenfeld, E. Boss, W. H. Slade,
636 *Biogeosciences* **6**, 947 (2009).
- 637 [6] A. Belcher, *et al.*, *Biogeosciences* **13**, 4927 (2016).
- 638 [7] M. H. Iversen, H. Ploug, *Biogeosciences* **7**, 2613 (2010).
- 639 [8] D. J. Clements, *et al.*, A new estimate of Global Ocean Carbon Flux from
640 In Situ Optical Observations and Supervised Learning (submitted). (2021).
- 641 [9] M.-I. Pujol, *et al.*, *Ocean Science* **12**, 1067 (2016).
- 642 [10] Ž. Kovač, T. Platt, S. Sathyendranath, *ICES Journal of Marine Science*
643 **78**, 1398 (2021).
- 644 [11] H. A. Bouman, *et al.*, *Earth System Science Data* **10**, 251 (2018).
- 645 [12] N. O. B. P. Group, Modis-aqua level 3 mapped downwelling diffuse attenu-
646 ation coefficient data version r2018.0 (2017).
- 647 [13] L. Zhai, *et al.*, *Geophysical Research Letters* **35** (2008).
- 648 [14] F. Roquet, G. Madec, T. J. McDougall, P. M. Barker, *Ocean Modelling* **90**,
649 29 (2015).
- 650 [15] M. Picheral, *et al.*, *Limnology and Oceanography: Methods* **20**, 115 (2022).
- 651 [16] G. Dall'Olmo, K. A. Mork, *Geophysical Research Letters* **41**, 2921 (2014).
- 652 [17] R. Sauzède, J. E. Johnson, H. Claustre, G. Camps-Valls, A. B. Ruescas,
653 *ISPRS Annals of the Photogrammetry, Remote Sensing and Spatial Infor-
654 mation Sciences* **V-2-2020**, 949 (2020).
- 655 [18] R. Kiko, *et al.*, *Nature Geoscience* **10**, 852 (2017).
- 656 [19] C. B. Mouw, A. Barnett, G. A. McKinley, L. Gloege, D. Pilcher, *Earth
657 System Science Data* **8**, 531 (2016).

658 **5 Supplementary Material**

685 **5.1 Eddy merging**

686 Temperature increased along 1026.80 (from xx to yy°) and 1027.20 kg/m³ (from
687 xx to yy°) isopycnals between the 13 April and the 23 September 2021 (upper
688 panels of Supplementary Figure S4). During the same period, salinity decreased
689 of xx g/kg between 500–600 m (lower panel of Supplementary Figure S4).



662 Figure S1: ADCP results. To write
660

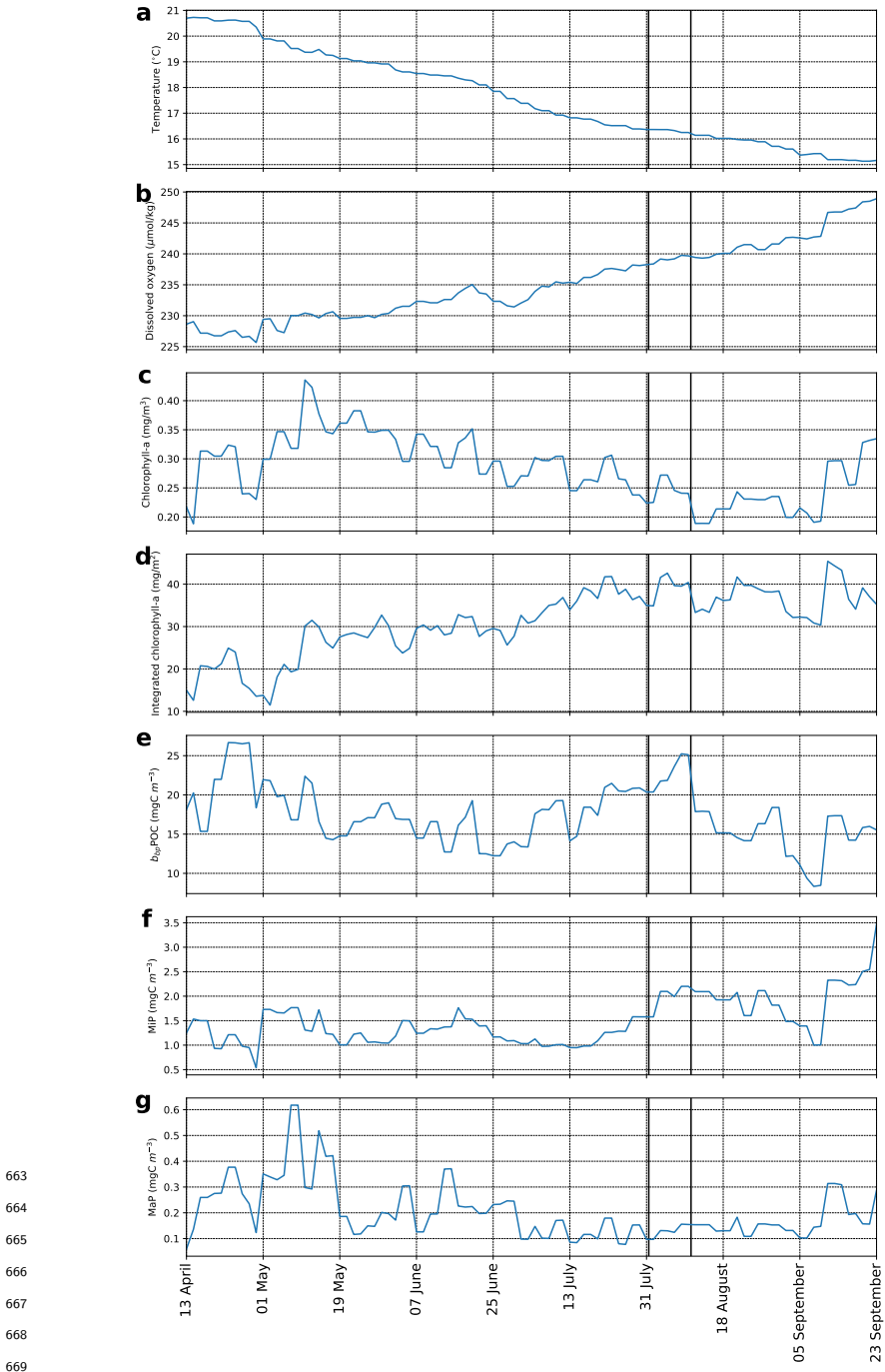
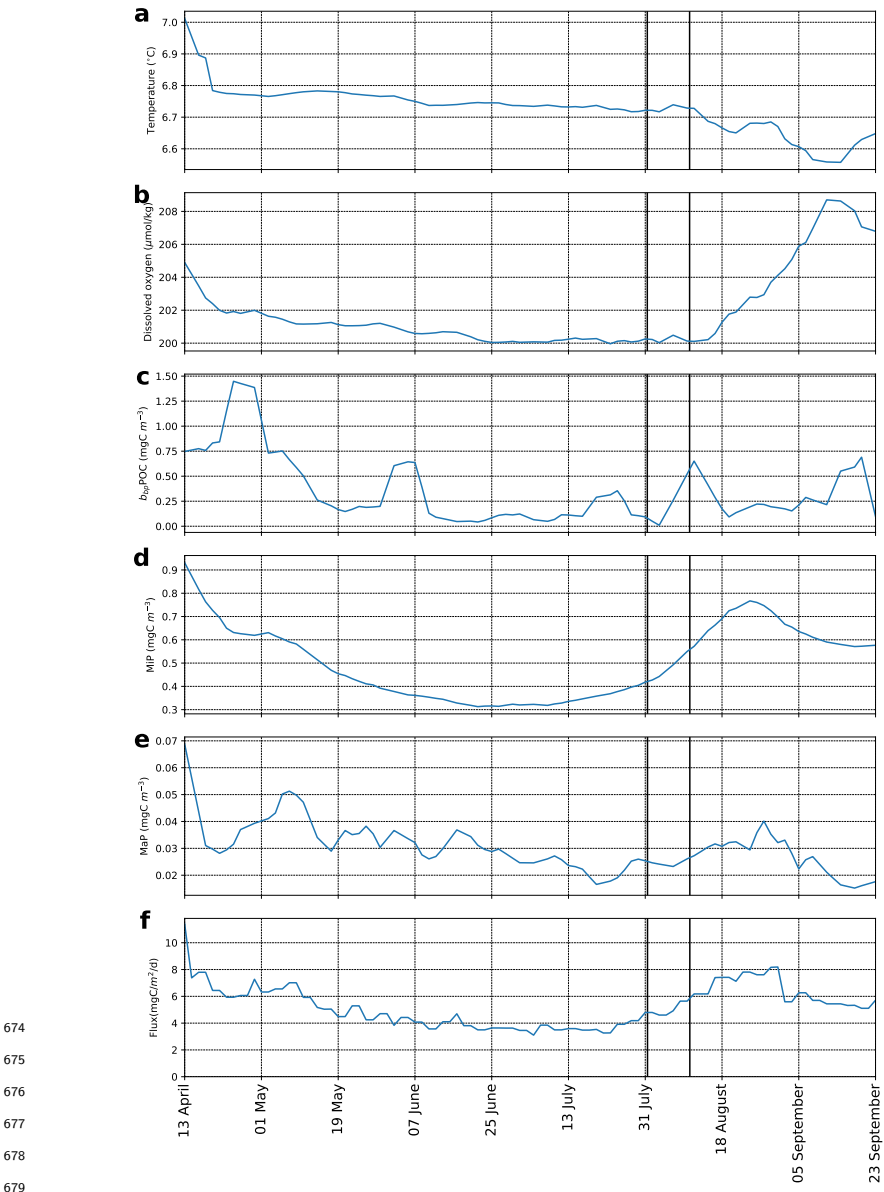
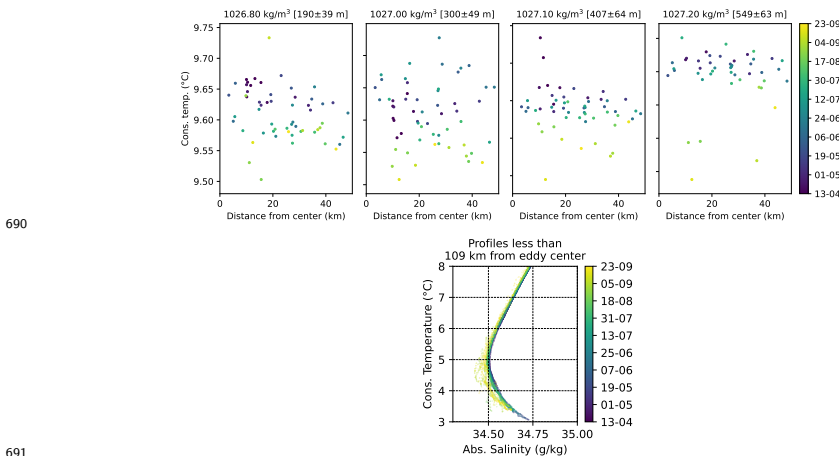


Figure S2: Time series of mean temperature (panel a), dissolved oxygen (panel b), chlorophyll *a* (panel c), integrated chlorophyll *a* (panel d), $b_{bp}\text{POC}$ (panel e), MiP POC (panel f), and MaP POC (panel g), in the mixed layer depth.



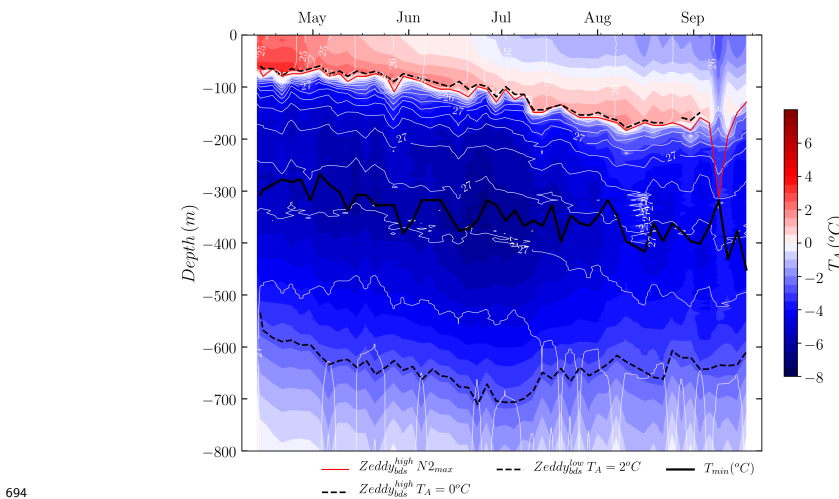
680 Figure S3: Time series of mean temperature (panel **a**), dissolved oxygen (panel
 681 **b**), $b_{bp}\text{POC}$ (panel **c**), MiP POC (panel **d**), MaP POC (panel **e**), and POC flux
 682 (panel **f**), in the eddy core (defined as the layer between 1026.82–1027.24 kg/m^3
 683 isopycnals, Fig. 2b).



690
691

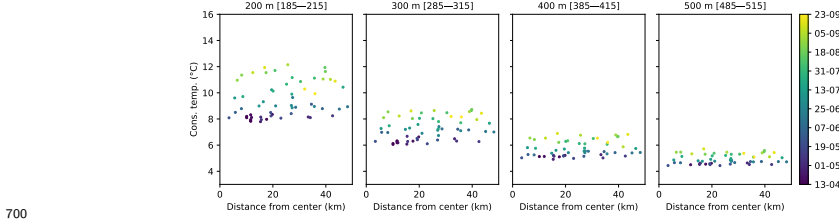
692

Figure S4: to write.

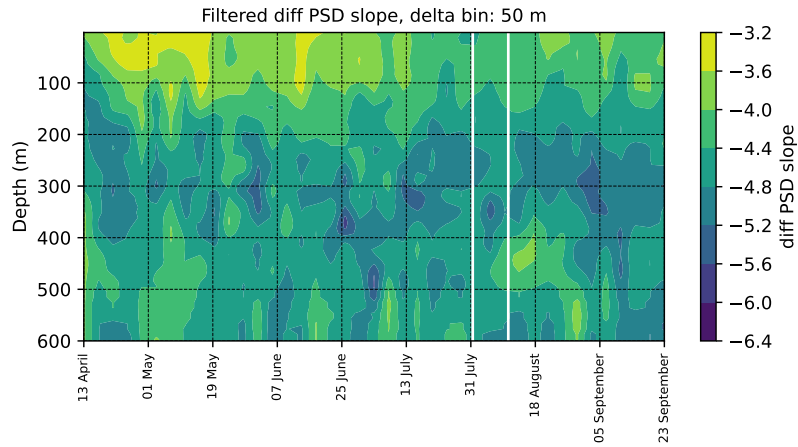


694

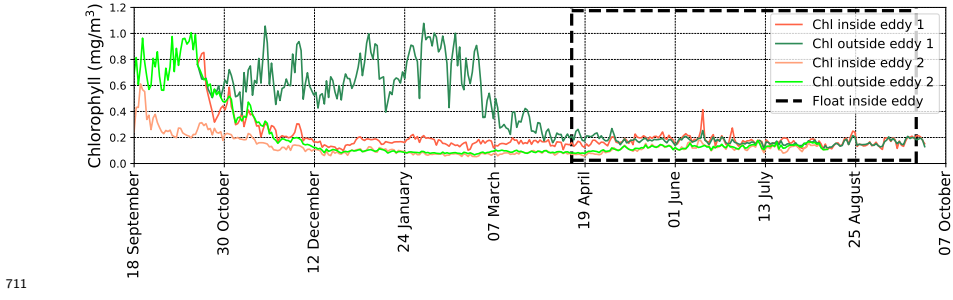
695 Figure S5: Temperature anomaly as a function of time and depth. For each pro-
696 file, the temperature anomaly was obtained by subtracting the float-measured
697 temperature to the global temperature climatology obtained from the World
698 Ocean Atlas (WOA; <https://www.ncei.noaa.gov/products/world-ocean-atlas>)



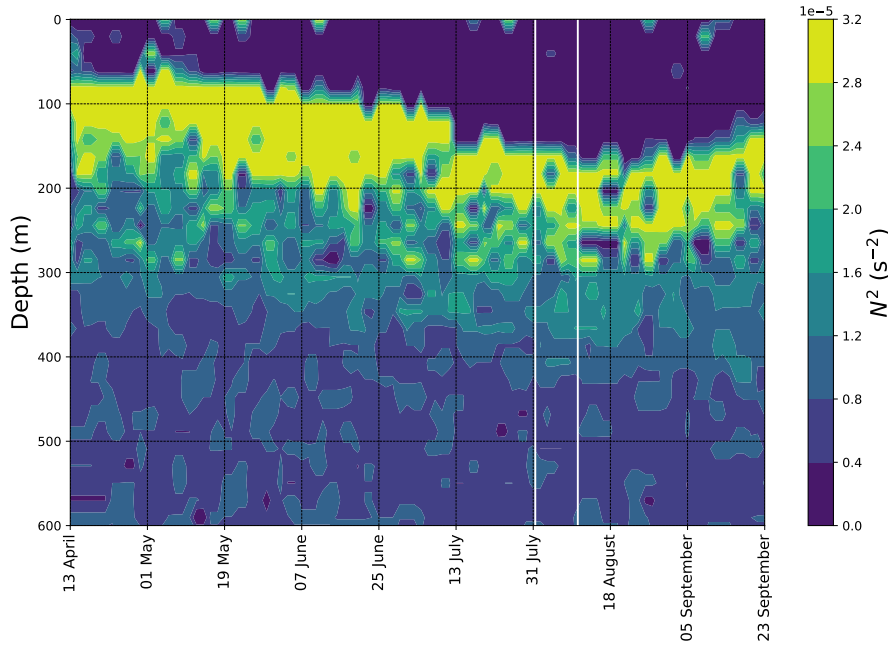
702 Figure S6: to write.



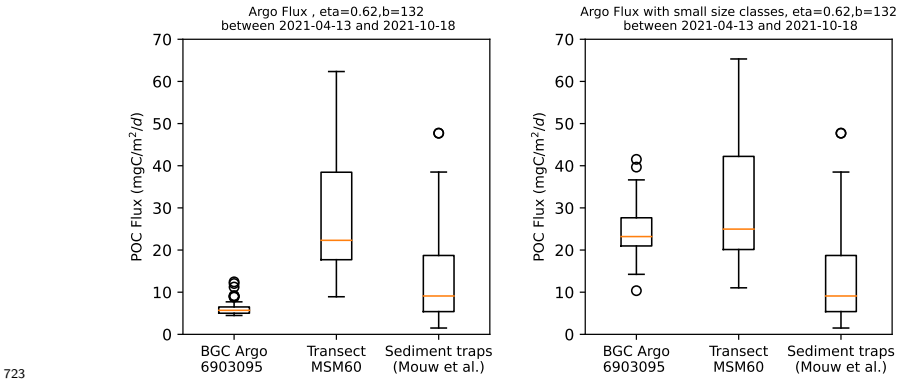
704 Figure S7: Slope of the particle size distribution (PSD), calculated from
 705 the linear regression between particle concentration and size class, both log-
 706 transformed, for the size classes between 0.1–16 mm. The PSD slopes were
 707 filtered with a Savitzky–Golay filter (Python module `scipy`), averaged over bins
 708 of 50 m depth, and interpolated in time and depth with a resolution of one day
 709 and 10 meters using the grid data function (Python module `scipy`).



712 Figure S8: Time series of the average satellite-derived chlorophyll *a* concentration
 713 inside and outside Eddy 1 and 2. The chlorophyll *a* concentration outside
 714 the eddies was calculated in a region identified as a circle around the eddy center,
 715 with a radius of ~ 380 km, minus the eddy surface area (Methods 4.1 and
 716 4.2). The region inside the black dashed line indicates the time period during
 717 which the BGC Argo float was trapped inside the eddy.
 718

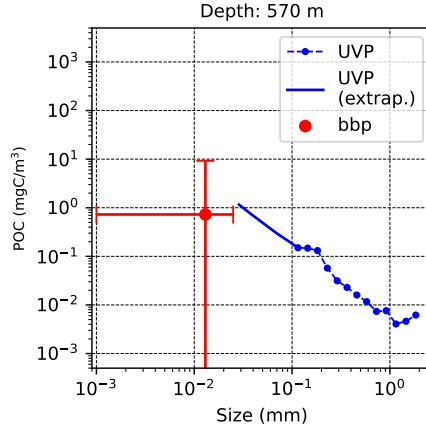


720 Figure S9: Brunt-Väisälä frequency as a function of time and depth, calculated
 721 using the Nsquared function (Python module gsw)



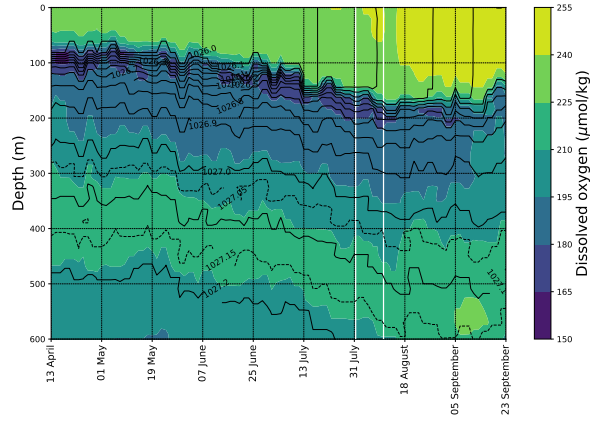
727 Figure S10: Panel **a**: box plot of the POC flux calculated at 600 m depth using
 728 (i) the BGC Argo float 6903095 (left box). The POC flux was calculated using
 729 all the profiles between the 4 April and the 18 October 2021; (ii) the POC flux
 730 measured during the sn202_msrm060 cruise (project uvp5_sn202_msrm060_filtered
 731 231; center box) which crossed our study region in 2017 (only profiles between
 732 10°E and 20°E were considered). Data were downloaded from Ecopart website
 733 (<https://ecopart.obs-vlfr.fr/>); (iii) sediment trap measurements from our study
 734 region obtained at (20.047°S, 9.200°E), (20.050°S, 9.150°E), and (20.047°S,
 735 9.155°E) (ref. [19]; right box). Panel **b** shows the same quantities reported
 736 in panel **a**, with the difference that the POC fluxes for cases (i) and (ii) were
 737 calculated including the extrapolated particle concentrations for the size classes
 738 between 0.025–0.1 mm (MM 4.3). Statistical differences between the POC flux
 739 values were tested with a Mann Whitney U test (mannwhitneyu function from
 740 Python module scipy). Left box was significantly similar to center box in panel
 741 b (p-value=0.12).

742 The problem here is that, using the classic eta and b values (0.62 and 132
 743 respect.), the POC fluxes are always significantly different from in situ trap
 744 measurements. With b=66, they were much more similar



747

748 Figure S11: POC concentration (y -axis) as a function of the size class con-
 749 sidered (x -axis) at a depth of 570 m, averaged between the 4 April and the
 750 19 August 2021. Both axes are in logarithmic scale. POC concentration val-
 751 ues were obtained from the particle concentrations directly measured by the
 752 UVP6 (size classes between 0.102–16.40 mm; blue dashed line with dots)
 753 and extrapolated (size classes between 0.025–0.102 mm; solid blue line). The red
 754 dot shows the b_{bp} POC with the associated uncertainties (standard deviation,
 755 y -axis; 0.001–0.025 mm, x -axis).



757

758 Figure S12: Dissolved oxygen as a function of time and depth, with superposed
 759 isopycnal contour lines (black lines).

761

762 Figure S13: Apparent oxygen utilisation (AOU) in the mixed layer as a function
763 of time.

